SUPPLEMENTARY INFORMATION

Binding and separation of CO_2, SO_2 and C_2H_2 in homo- and hetero-metallic metal-organic framework materials

Lydia Briggs,[1#] Ruth Newby,[2#] Xue Han,[1] Christopher G. Morris,[1,3] Mathew Savage,[1] Cristina Perez Krap[2], Timothy L. Easun,[4] Mark D. Frogley,[3] Gianfelice Cinque,[3] Claire A. Murray,[3] Chiu C. Tang,[3] Junliang Sun,[5] Sihai Yang[1]* and Martin Schröder[1]*

[1] School of Chemistry, University of Manchester, Oxford Road, Manchester, M13 9PL (UK)

[2] School of Chemistry, University of Nottingham, University Park, Nottingham, NG7 2RD (UK)

[3] Diamond Light Source, Harwell Science Campus, Oxfordshire, OX11 0DE (UK)

[4] School of Chemistry, Cardiff University, Cardiff, CF10 3AT (UK)

[5] College of Chemistry and Molecular Engineering, Peking University, Beijing, 100871 (China)

# These authors contributed equally to the work.

Contents for Supplementary Information

1 Materials and methods

1.1 Chemicals

All chemicals were used as purchased without further purification. H_4L was synthesised from previously reported literature method.[1]

1.2 FT-IR spectroscopy

Infrared spectroscopic measurement on MFM-300(Al), MFM-300(Cr) and MFM-300($Al_{0.67}Cr_{0.33}$) and CO_2-loaded MFM-300($Al_{0.67}Cr_{0.33}$) were carried out on beamline B22 at Diamond Light Source using a Bruker Hyperion3000 microscope equipped with an LN2-cooled MCT (Mercury Cadmium Telluride) detector, coupled to a Bruker Vertex spectrometer. Experiments were carried out using a Linkam FTIR600 environmental gas stage using custom gas handling equipment at a constant flow rate of 100 cm^3 min^{-1}. The desolvated sample was generated *in situ* by heating the sample to 393 K under a flow of dry He for 2 h. The sample was then cooled to 298 K and dosed with freshly prepared analyte gas mixtures. CO_2 was dosed into the cell using mass flow controllers at the designed partial pressure, and the remaining flow was made up by an inert carrier gas. This was attached to the cell and then allowed to flow into a COSHH extractor, creating an open set up with a pressure of 1 bar maintained throughout the experiment. Due to the high intensity of the fundamental stretches of CO_2, this experiment focussed on the ν(OH) stretch and the combination bands of CO_2.

1.3 Synchrotron PXRD measurements

High-resolution X-ray powder diffraction of activated, CO_2-, C_2H_2- and SO_2-loaded MFM-300(Cr) and MFM-300($Al_{0.67}Cr_{0.33}$) was carried out on beamline I11 of the Diamond Light Source. A high brightness monochromatic beam was produced by a Si(111) monochromator and double-bounce harmonic rejection mirrors. The beam was delivered to the main instrument hutch where five multi-analysing crystal-detectors (MAC) travel in an arc of 2θ around the sample. Measurements were carried out in capillary mode and the sample environment controlled using an Oxford Cryosystems open-flow N_2 gas cryostat. The samples were ground to provide a uniform particle size, packed into a borosilicate capillary and mounted into a gas cell for *in situ* gas dosing. The sample was activated under vacuum (1 x 10^{-6} mbar) at 393 K for > 3 h to remove residual solvent molecules from the material. Diffraction data for the activated sample were collected and analysed to confirm that no residual solvent molecules are present in the pores. A gas dosing panel was used for *in situ* dosing of activated MFM-300(Cr) and activated MFM-300($Al_{0.67}Cr_{0.33}$) with 1 bar of gas (CO_2, C_2H_2 or SO_2). Wavelength and capillary details are tabulated in Tables S1 and S2. Additional activated and gas-loaded diffraction data for MFM-300(Cr) and MFM-300($Al_{0.67}Cr_{0.33}$) are shown in Figures S12-19.

1.4 TGA and ICP-OES measurements

Thermogravimetric analysis was carried out under a flow of air (5 mL min^{-1}) at a heating rate of 2 °C min^{-1} on a Perkin-Elmer Pyris1 Thermogravimetric analyser. Elemental analysis for C, H and N content of materials

was carried out using a CE-440 Elemental Analyser manufactured by Exeter Analytical. ICP-OES measurements were carried out using a Perkin-Elmer Optima 2000. TGA data for MFM-300(Cr) and MFM-300($Al_{0.67}Cr_{0.33}$) are shown in Figure S1.

1.5 Gas sorption measurements

Gas adsorption data were obtained by gravimetric methods using an IGA or a Xemis Instruments at the University of Manchester. Isotherms recorded from 273-303 K were measured using a Grant Optima TX150 water bath. All gases were ultra-pure research grade (99.999 %) purchased from BOC or AIRLIQUIDE. BET surface areas were calculated from CO_2 adsorption at 195 K using DFT/Monte Carlo methods. Before carrying out gas adsorption isotherms, a sample (~100 mg) was loaded onto the IGA or Xemis Instrument and degassed at 393 K under high vacuum (10^{-7} bar) for > 4 h to give fully desolvated material. Additional isotherms are shown in Figures S4 and S5.

1.6 Fitting of isotherm data to the Dual-Site Langmuir-Freundlich Model

Adsorption isotherms of CO_2, C_2H_2 and SO_2 in MFM-300(Cr) and MFM-300($Al_{0.67}Cr_{0.33}$) were fitted using the dual-site Langmuir-Freundlich model (Equation 1), where n is the amount adsorbed in mmol g^{-1}, P is the pressure in bar, q_{sat} is the saturation capacity in mmol g^{-1}, b_1 is the Langmuir parameter in bar^{-1}, and v_1 is the Freundlich parameter for two sites 1 and 2. All values for R^2 are > 0.9 confirming a good fit to the model. Fittings for MFM-300(Cr) and MFM-300($Al_{0.67}Cr_{0.33}$) are shown in Figures S6-S8 for MFM-300(Cr) and Figures S9-S11 for MFM-300($Al_{0.67}Cr_{0.33}$).

$$n = \frac{q_{sat_1} b_1 P^{v_1}}{1 + b_1 P^{v_1}} + \frac{q_{sat_2} b_2 P^{v_2}}{1 + b_2 P^{v_2}} \qquad (1)$$

1.7 Analysis and derivation of selectivity using Ideal Adsorption Solution Theory (IAST)

Ideal adsorbed solution theory (IAST)[2] was used to determine the selectivity factor, S, for binary mixtures using pure component isotherm data; x_i is the amount of each component adsorbed as determined from IAST and y_i is the mole fraction of each component in the gas phase at equilibrium (Equation 2).

$$S = \frac{\frac{x_1}{y_1}}{\frac{x_2}{y_2}} \qquad (2)$$

1.8 Analysis and derivation of the isosteric heats of adsorption for adsorption of CO_2, C_2H_2 and SO_2 in MFM-300(Cr) and MFM-300($Al_{0.67}Cr_{0.33}$)

Isotherms at 273-303 K were used to estimate the isosteric enthalpies (ΔH) for CO_2, C_2H_2 and SO_2 in MFM-300(Cr) and MFM-300($Al_{0.67}Cr_{0.33}$), and were fitted to the Van't Hoff equation (3);

$$lnP = -\frac{\Delta H}{RT} + \frac{\Delta S}{R} \qquad (3)$$

where P is pressure, T is the temperature, and R is the ideal gas constant. All linear fittings show R^2 greater than 0.99 confirming consistency of the isotherm data to the fitting. These results have been summarized in Tables S4-S6 for MFM-300(Cr) and Tables S7-S9 for MFM-300($Al_{0.67}Cr_{0.33}$).

2. Synthesis and structures of MFM-300(Cr) and MFM-300($Al_{0.67}Cr_{0.33}$)

$CrCl_3 \cdot 6H_2O$ (283 mg, 1.06 mmol) and H_4L (70 mg, 0.212 mmol) were dissolved in water (10 mL) to which hydrochloric acid (12 %, 1.5 mL) was then added. The reaction mixture was transferred to a 23 mL autoclave which was sealed and heated to 210 °C for 72 h. The resulting blue powder was separated by filtration and washed repeatedly with acetone and stored in acetone until required. Yield: 91 mg, 92 %.

$AlCl_3.6H_2O$ (171 mg, 0.708 mmol), $CrCl_3 \cdot 6H_2O$ (94.3 mg, 0.354 mmol) and H_4L (70 mg, 0.212 mmol) was dissolved in water (10 mL) to which hydrochloric acid (12 %, 1.5 mL) was then added. The reaction mixture was transferred to a 23 mL autoclave which was sealed and heated to 210 °C for 72 h. The resulting light-blue powder was separated by filtration and washed repeatedly with acetone and stored in acetone until required. Yield: 78 mg, 86 %.

2.1 Crystal structures of MFM-300(Cr) and of guest-loaded MFM-300(Cr)

Crystal data for MFM-300(Cr), $[Cr_2(OH)_2(C_{16}H_6O_8]$ activated. Blue powder. Tetragonal, space group I_4122, $a = b = 14.99047(3)$ Å, $c = 11.99050(3)$ Å, $V = 2694.436(13)$ Å^3, $M = 463.89$, $T = 273$ K, $Z = 4$. The final Rietveld plot corresponds to satisfactory crystal structure model and profile indicators ($R_p = 3.76$ % and $R_{wp} = 5.37$ %) with a goodness-of-fit parameter of 2.00.

Crystal data for MFM-300(Cr).$4CO_2$ $[Cr_2(OH)_2(C_{16}H_6O_8)](CO_2)_4$. Blue powder. Tetragonal, space group I_4122, $a = b = 14.99472(3)$ Å, $c = 11.98653(3)$ Å, $V = 2695.069(14)$ Å^3, $M = 639.85$, $T = 195$ K, $Z = 4$. The final Rietveld plot corresponds to satisfactory crystal structure model and profile indicators ($R_p = 3.32$ % and $R_{wp} = 2.43$ %) with a goodness-of-fit parameter of 1.89.

Crystal data for MFM-300(Cr)·$4SO_2$. $[Cr_2(OH)_2(C_{16}H_6O_8)](SO_2)_4$. Blue powder. Tetragonal, space group I_4122, $a = b = 15.00063(4)$ Å, $c = 11.98684(3)$ Å, $V = 2697.265(17)$ Å^3, $M = 719.74$, $T = 273(2)$ K, $Z = 4$. The final Rietveld plot corresponds to satisfactory crystal structure model and profile indicators ($R_p = 4.01$% and $R_{wp} = 5.28$%) with a goodness-of-fit parameter of 2.07.

Crystal data for MFM-300(Cr)·$4C_2H_2$. $[Cr_2(OH)_2(C_{16}H_6O_8)](C_2H_2)_4$. Blue powder. Tetragonal, space group I_4122, $a = b = 14.98903(4)$ Å, $c = 11.98093(3)$ Å, $V = 2691.768(15)$ Å^3, $M = 567.96$, $T = 273(2)$ K, $Z = 4$. The final Rietveld plot corresponds to satisfactory crystal structure model and profile indicators ($R_p = 5.05$% and $R_{wp} = 6.98$%) with a goodness-of-fit parameter of 2.38.

Table S1: Crystallographic information for desolvated CO_2, SO_2 and C_2H_2 loaded MFM-300(Cr)

	$[Cr_2C_{16}O_{10}H_8]$	MFM-300(Cr).4CO_2	MFM-300(Cr).4SO_2	MFM-300(Cr).4C_2H_2
Empirical formula	$[Cr_2C_{16}O_{10}H_8]$	$[Cr_2C_{16}O_{10}H_8].(CO_2)_4$	$[Cr_2C_{16}O_{10}H_8].(SO_2)_4$	$[Cr_2C_{16}O_{10}H_8].(C_2H_2)_4$
M_r	464.22	640.26	720.46	568.38
Crystal System	Tetragonal	Tetragonal	Tetragonal	Tetragonal
Space Group	$I4_1\,22$	$I4_1\,22$	$I4_1\,22$	$I4_1\,22$
Temperature	293 K	195 K	293 K	293 K
a = b / Å	14.99047(32)	14.99472(3)	15.00063(4)	14.98903(4)
c / Å	11.990498(26)	11.98653(3)	11.98684(3)	11.98093(3)
V / Å^3	2694.436(13)	2695.069(14)	2697.265(17)	2691.768(15)
Capillary Diameter	0.74919 mm	0.63465	0.7 mm	0.74048 mm
Radiation type	Synchrotron Monochromatic X-ray	Synchrotron Monochromatic X-ray	Synchrotron Monochromatic X-ray	Synchrotron Monochromatic X-ray
Wavelength	0.825687	0.825687	0.825687	0.825774
Scan type	Continuous	Continuous	Continuous	Continuous
Refinement Method	Rietveld	Rietveld	Rietveld	Rietveld
R_{exp}	2.70	2.43	2.55	2.93
R_{wp}	5.37	4.59	5.28	6.98
R_p	3.76	3.32	4.01	5.05
GoF	2.00	1.89	2.07	2.38

2.2 Crystal structures of MFM-300($Al_{0.67}Cr_{0.33}$) and guest-loaded MFM-300($Al_{0.67}Cr_{0.33}$)

Crystal data for MFM-300($Al_{0.67}Cr_{0.33}$). $[Al_{1.33}Cr_{0.667}(OH)_2(C_{16}H_6O_8]$. Light blue powder. Tetragonal, space group I_4122, $a = b = 14.8655(2)$ Å, $c = 11.8656(3)$ Å, $V = 2622.03(10)$ Å^3, $M = 430.57$, $T = 273$ K, $Z = 4$. The final Rietveld plot corresponds to satisfactory crystal structure model and profile indicators ($R_p = 6.21$ and $R_{wp} = 8.40$) with a goodness-of-fit parameter of 2.78.

Crystal data for MFM-300($Al_{0.67}Cr_{0.33}$).4CO_2 $[Al_{1.33}Cr_{0.667}(OH)_2(C_{16}H_6O_8)](CO_2)_4$. Blue powder. Tetragonal, space group I_4122, $a = b = 14.8732(2)$ Å, $c = 11.8513(3)$ Å, $V = 2621.63(10)$ Å^3, $M = 597.73$, $T = 195$ K, $Z = 4$. The final Rietveld plot corresponds to satisfactory crystal structure model and profile indicators ($R_p = 5.94$ and $R_{wp} = 8.40$) with a goodness-of-fit parameter of 2.54.

Crystal data for MFM-300($Al_{0.67}Cr_{0.33}$)·4SO_2. $[Al_{1.33}Cr_{0.667}C_{16}O_{10}H_8].(SO_2)_4$. Blue powder. Tetragonal, space group I_4122, $a = b = 14.84914(4)$ Å, $c = 11.83263(4)$ Å, $V = 2697.265(17)$ Å^3, $M = 687.06$, $T = 273(2)$ K, $Z = 4$. The final Rietveld plot corresponds to satisfactory crystal structure model and profile indicators ($R_p = 4.50$ and $R_{wp} = 6.04$) with a goodness-of-fit parameter of 2.42.

Crystal data for MFM-300($Al_{0.67}Cr_{0.33}$)·2.325C_2H_2. $[Al_{1.33}Cr_{0.667}C_{16}O_{10}H_8].(C_2H_2)_{2.325}$. Blue powder. Tetragonal, space group I_4122, $a = b = 14.85452(2)$ Å, $c = 11.86691(6)$ Å, $V = 2618.467(17)$ Å^3, $M = 446.433$,

T = 273(2) K, Z = 4. The final Rietveld plot corresponds to satisfactory crystal structure model and profile indicators (R_p = 4.61 and R_{wp} = 6.28) with a goodness-of-fit parameter of 1.44.

Table S2: Crystallographic information for desolvated, CO_2-, SO_2- and C_2H_2-loaded MFM-300($Al_{0.67}Cr_{0.33}$)

	MFM-300($Al_{0.67}Cr_{0.33}$)	MFM-300($Al_{0.67}Cr_{0.33}$).4CO_2	MFM-300($Al_{0.67}Cr_{0.33}$).4SO_2	MFM-300($Al_{0.67}Cr_{0.33}$).2.325C_2H_2
Empirical formula	$[Al_{1.333}Cr_{0.666}C_{16}O_{10}H_8]$.	$[Al_{1.333}Cr_{0.666}C_{16}O_{10}H_8]$.$(CO_2)_4$	$[Al_{1.333}Cr_{0.666}C_{16}O_{10}H_8]$.$(SO_2)_4$	$[Al_{1.333}Cr_{0.666}C_{16}O_{10}H_8]$.$(C_2H_2)_{2.325}$
M_r	430.87	606.91	687.11	491.413
	Tetragonal	Tetragonal	Tetragonal	Tetragonal
Crystal System	$I4_1$ 22	$I4_1$ 22	$I4_1$ 22	$I4_1$ 22
Space Group	273 K	195 K	293 K	293 K
Temperature	14.8655(2)	14.8732(2)	14.84914(4)	14.85452(2)
a=b / Å	11.8656(3)	11.8513(3)	11.83263(4)	11.86691(6)
c / Å	2622.03(10)	2621.63(10)	2609.060(18)	2618.467(14)
V / $Å^3$	0.69954 mm	0.78 mm	0.7 mm	0.83855 mm
	Synchrotron Monochromatic X-ray	Synchrotron Monochromatic X-ray	Synchrotron Monochromatic X-ray	Synchrotron Monochromatic X-ray
Capillary Diameter	0.826651	0.826651	0.825687	0.825690
Radiation type	Synchrotron Monochromatic X-ray	Synchrotron Monochromatic X-ray	Synchrotron Monochromatic X-ray	Synchrotron Monochromatic X-ray
Wavelength	0.825690	0.825690	0.825690	0.825690
Scan type	Continuous	Continuous	Continuous	Continuous
Refinement Method	Rietveld	Rietveld	Rietveld	Rietveld
R_{exp}	3.03	3.05	2.49	4.37
R_{wp}	8.40	7.75	6.04	6.28
R_p	6.21	5.94	4.50	4.61
GoF	2.78	2.54	2.42	1.44

3. Characterisation

3.1 Unit cell parameters

Table S3: Unit cell parameters of MFM-300(Al), MFM-300(Cr) and MFM-300($Al_{0.67}Cr_{0.33}$).

	MFM-300(Al)	MFM-300(Cr)	MFM-300($Al_{0.67}Cr_{0.33}$)
*a = b (*Å)	14.82958(6)	14.99047(3)	14.8655(2)
*c (*Å)	11.77316(5)	11.99050(3)	11.8656(3)
Cell Volume ($Å^3$)	2589.11(3)	2694.44(1)	2622.03(1)

3.2 TGA

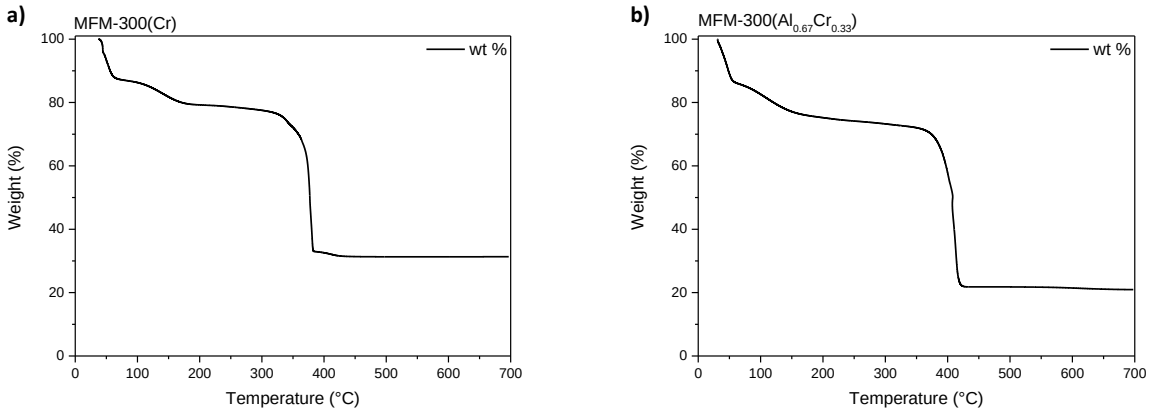

Figure S1: TGA of a) MFM-300(Cr) and b) MFM-300($Al_{0.67}Cr_{0.33}$) under air using a temperature ramp of 2 °C min^{-1} between 30-700 °C. A 28 % solvent loss is observed for MFM-300(Cr) attributed to loss of acetone and water from pores. Decomposition is observed at ~320-375 °C. The residual 33 % of mass is attributed to Cr_2O_3. A 28% solvent loss is observed for MFM-300($Al_{0.67}Cr_{0.33}$) attributed to loss of acetone and water from pores. Decomposition is is observed above 340 °C. The residual 22 % of mass is attributed to a mixture of Cr_2O_3 and Al_2O_3.

3.3 PXRD characterisation

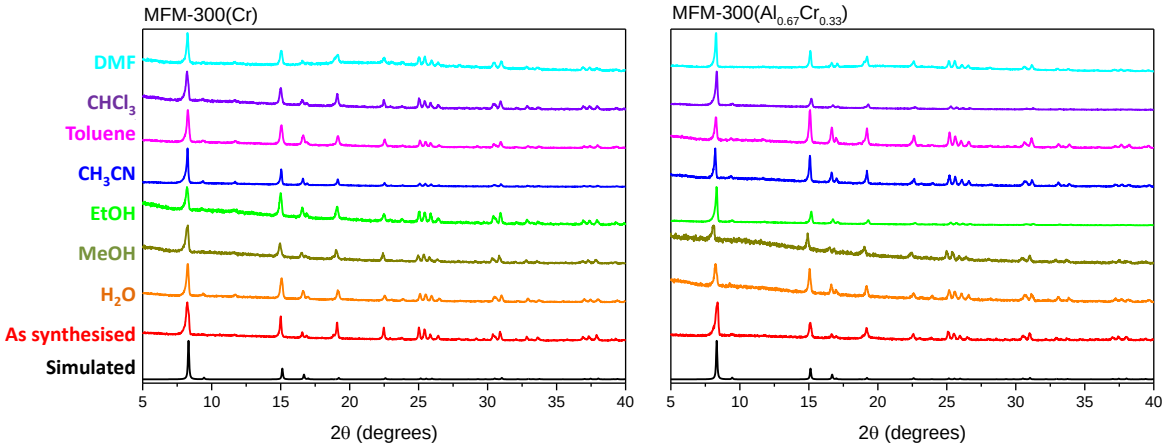

Figure S2: PXRD diffractograms confirming the stability of MFM-300(Cr) and MFM-300($Al_{0.67}Cr_{0.33}$) to common laboratory solvents [λ = 1.54056(2) Å].

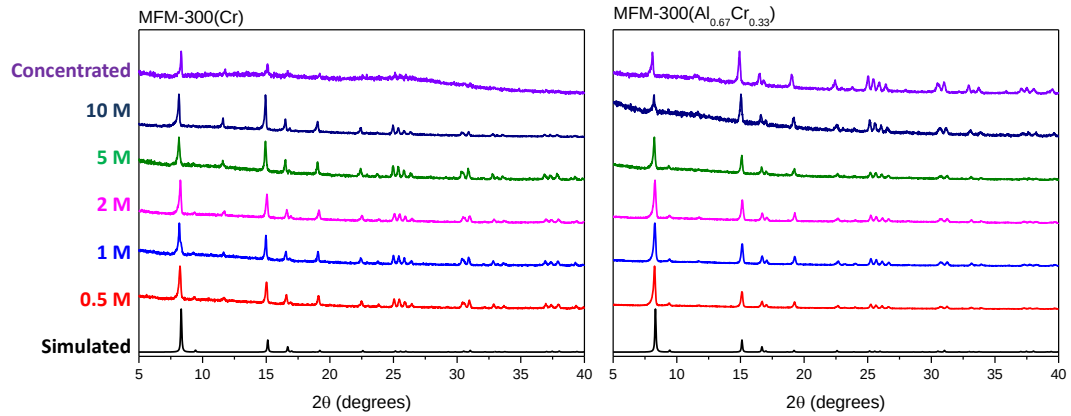

Figure S3: PXRD diffractograms showing the stability of MFM-300(Cr) and MFM-300($Al_{0.67}Cr_{0.33}$) to various molarities of H_2SO_4 for 30 mins and washed with water [λ = 1.54056(2) Å].

3.4 ICP-OES results

Anal. Calcd. (Found) for $[Cr_2(OH)_2(C_{16}H_6O_8)].5H_2O$: Cr 18.8 (19.2); C 34.7 (32.8); H 3.27 (3.85); N 0.00 (0.00).

Anal. Calcd. (Found) for $[Al_{1.33}Cr_{0.67}(OH)_2(C_{16}H_6O_8)].2((CH_3)_2CO).2(H_2O)$: Cr 5.95, (6.26); Al 6.17 (5.59); C 45.3 (45.6); H 4.15 (4.01); N 0.00 (0.00).

3.5 Gas adsorption isotherms for MFM-300(Cr)

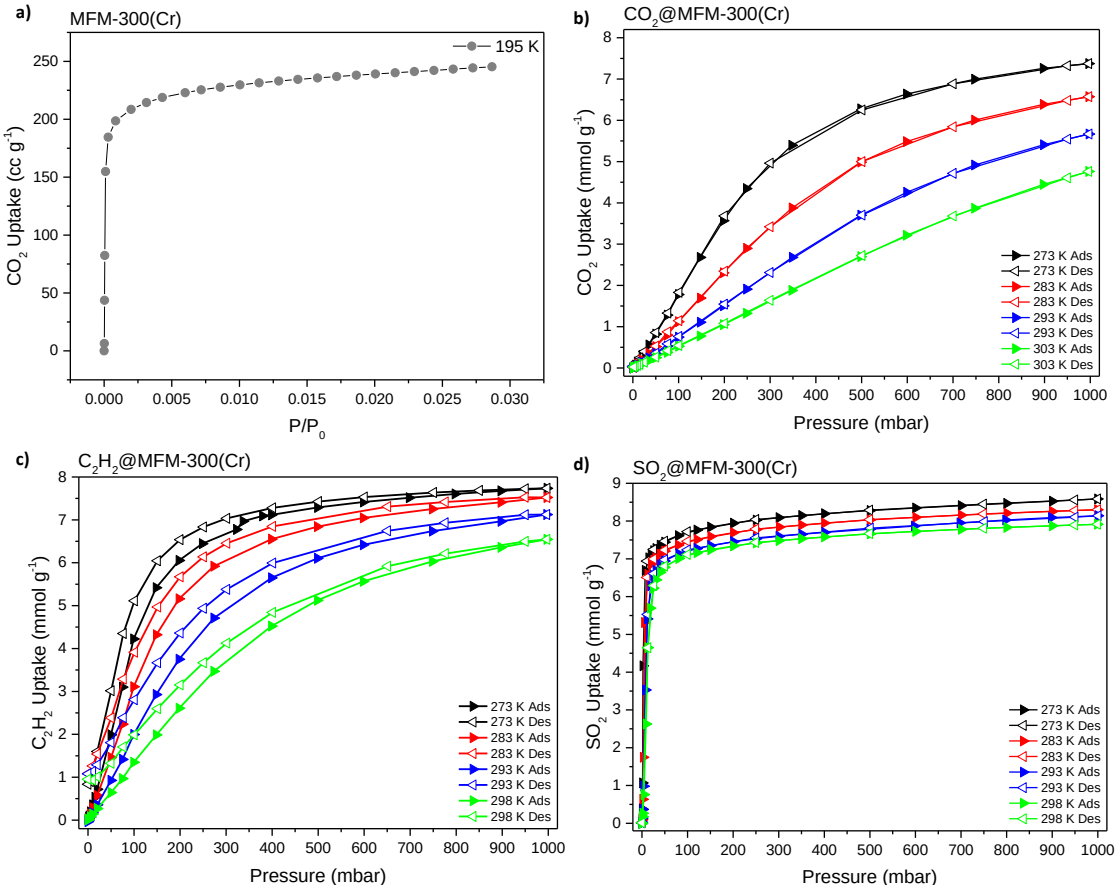

Figure S4: Gas isotherms for MFM-300(Cr). a) CO_2 at 195 K; b) CO_2 at 273-303 K to 1 bar; c) C_2H_2 at 273-303 K to 1 bar; d) SO_2 at 273-303 K to 1 bar.

3.6 Gas Adsorption isotherms for MFM-300($Al_{0.67}Cr_{0.33}$)

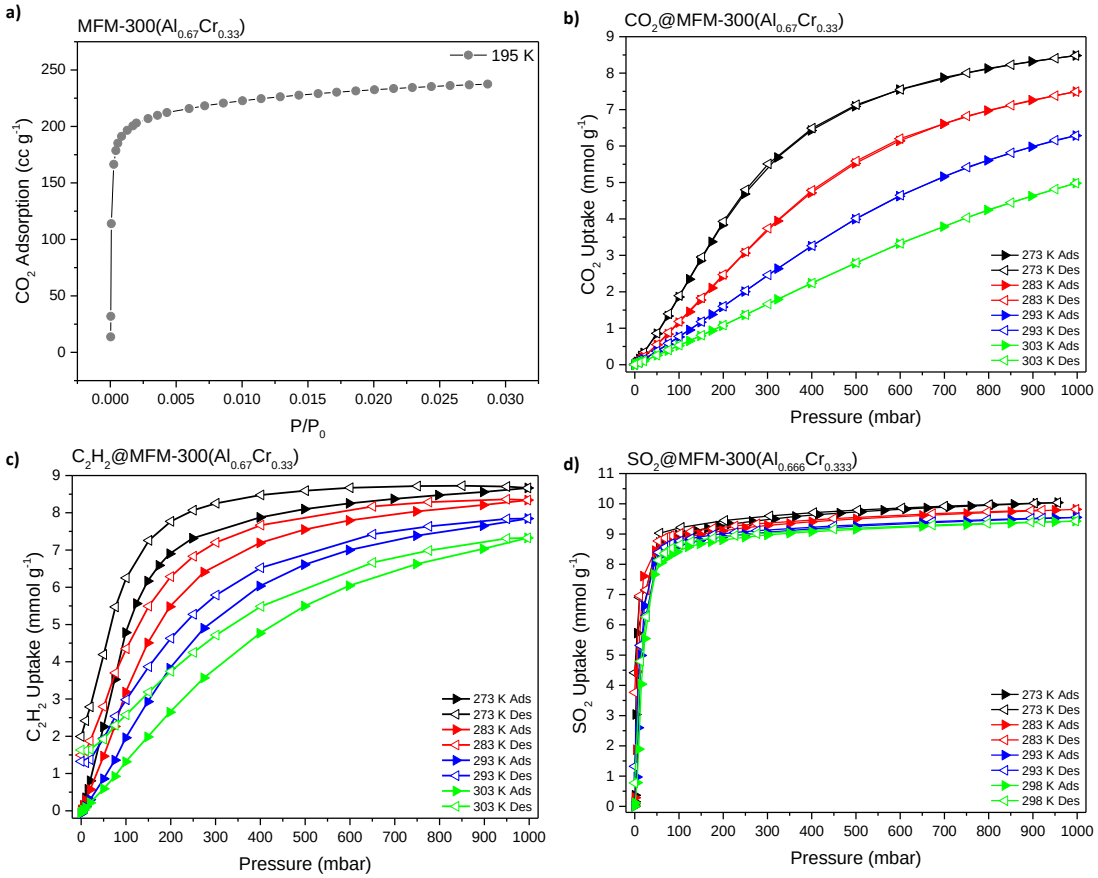

Figure S5: Gas isotherms for MFM-300($Al_{0.67}Cr_{0.33}$). a) CO_2 at 195 K; b) CO_2 at 273-303 K to 1 bar; c) C_2H_2 at 273-303 K to 1 bar; d) SO_2 at 273-303 K to 1 bar.

3.7 Fitting of isotherms to the Dual-Site Langmuir Equation - MFM-300(Cr)

CO_2@MFM-300(Cr)

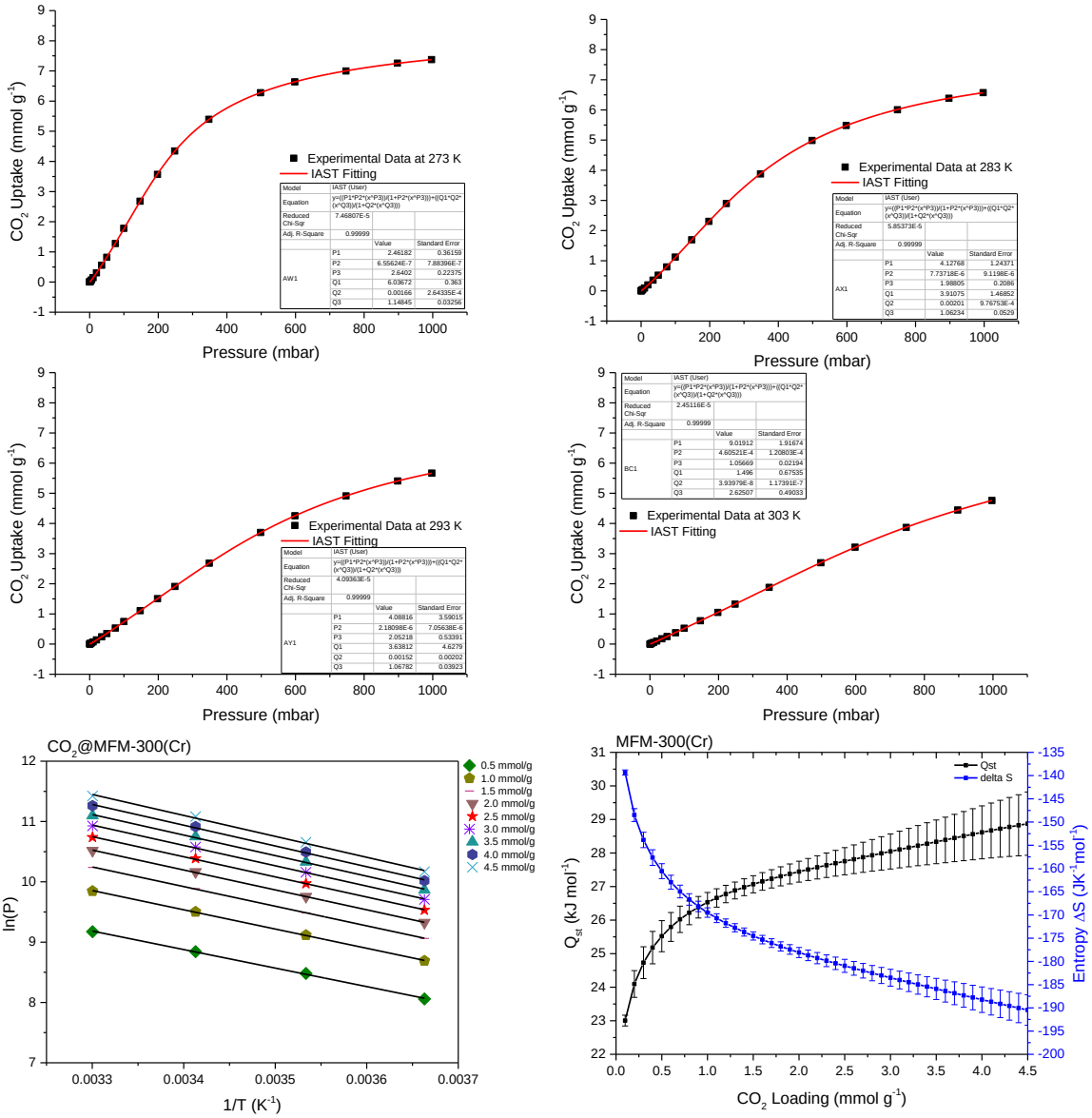

Figure S6: Fitting of isotherm by Dual-Site Langmuir Freundlich model for CO_2-loaded MFM-300(Cr) at 273, 283, 293 and 303 K to 1 bar. Van't Hoff linear fittings and respective plots for Q_{st} and ΔS.

Table S4: Thermodynamic parameters for CO_2 adsorption in MFM-300(Cr)

n mmol g^{-1}	Q_{st} kJ mol^{-1}	Q_{st} error kJ mol^{-1}	ΔS J K^{-1} mol^{-1}	ΔS error J K^{-1} mol^{-1}	R^2
0.5	25.52118	0.46312	-160.5759	1.61171	0.99901
1.0	26.5307	0.29342	-169.49121	1.02113	0.99963
1.5	27.06919	0.25514	-174.52116	0.8879	0.99973
2.0	27.44352	0.31219	-178.08031	1.08646	0.99961
2.5	27.75531	0.40493	-180.9627	1.4092	0.99936
3.0	28.04652	0.52178	-183.51865	1.81586	0.99896
3.5	28.33347	0.65196	-185.91946	2.26889	0.99841
4.0	28.61557	0.78985	-188.23813	2.74877	0.99772
4.5	28.87403	0.94366	-190.46686	3.28404	0.9968

C_2H_2@MFM-300(Cr)

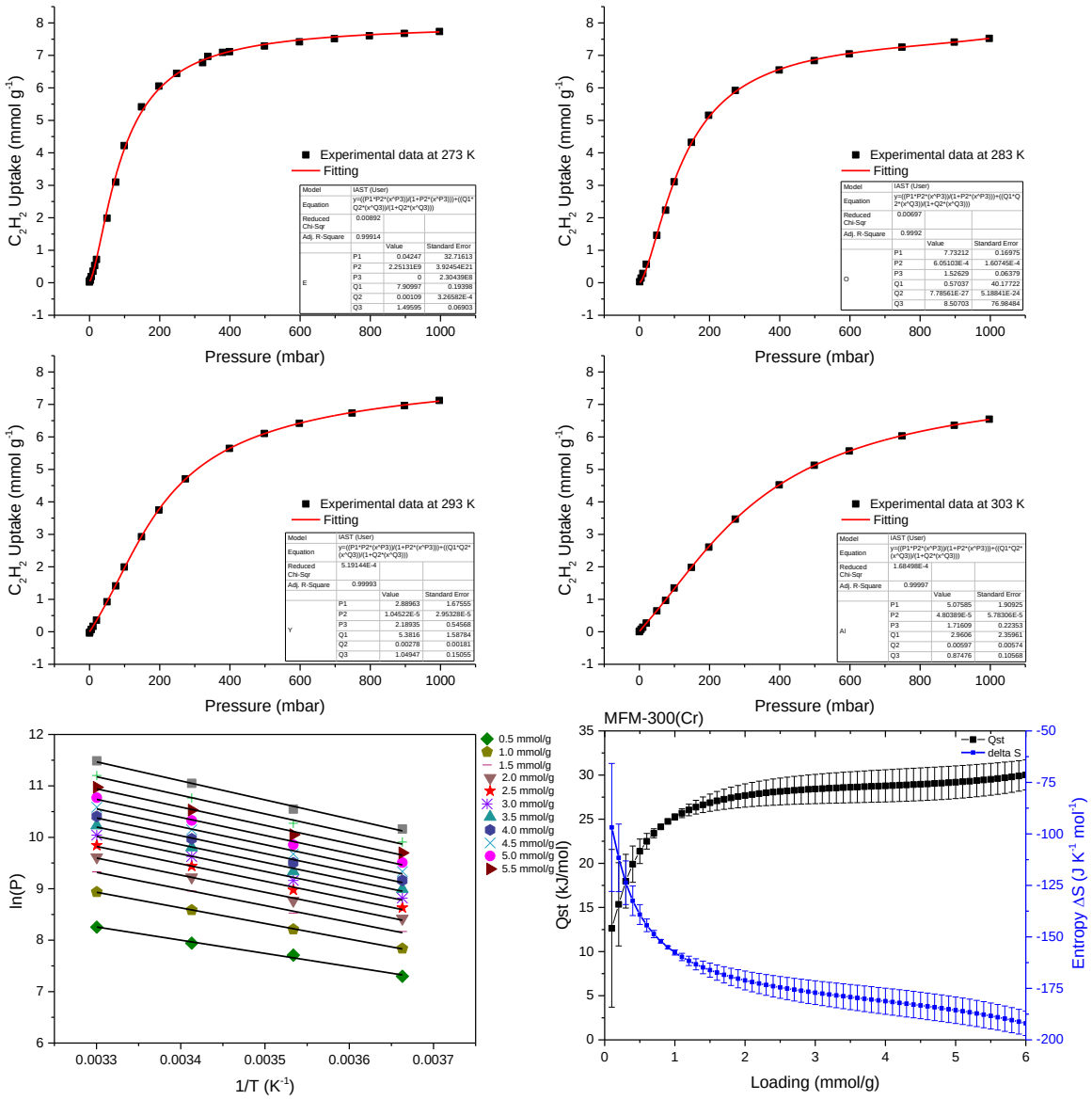

Figure S7: Fitting of isotherm by Dual-Site Langmuir Freundlich model for C_2H_2-loaded MFM-300(Cr) at 273, 283, 293 and 303 K up to 1 bar. Van't Hoff linear fittings and respective plots for Q_{st} and ΔS.

Table S5: Thermodynamic parameters for C_2H_2 adsorption in MFM-300(Cr)

n mmol g^{-1}	Q_{st} kJ mol^{-1}	Q_{st} error kJ mol^{-1}	ΔS J K^{-1} mol^{-1}	ΔS error J K^{-1} mol^{-1}	R^2
0.5	42.76913	6.46541	-212.39394	22.50023	0.93444
1.0	33.71578	1.88841	-187.31001	6.57184	0.99065
1.5	33.10992	1.38982	-188.41801	4.83672	0.99473
2.0	33.32941	1.15605	-191.44102	4.02318	0.9964
2.5	33.70356	0.96012	-194.57236	3.34129	0.99757
3.0	34.11143	0.78571	-197.61064	2.73435	0.99841
3.5	34.53119	0.64205	-200.60343	2.23441	0.99896
4.0	34.9666	0.547	-203.65568	1.90362	0.99927
4.5	35.43081	0.52795	-206.90581	1.83733	0.99933
5.0	35.94318	0.62825	-210.54631	2.18637	0.99908
5.5	36.53147	0.9261	-214.89199	3.22293	0.99807

SO_2@MFM-300(Cr)

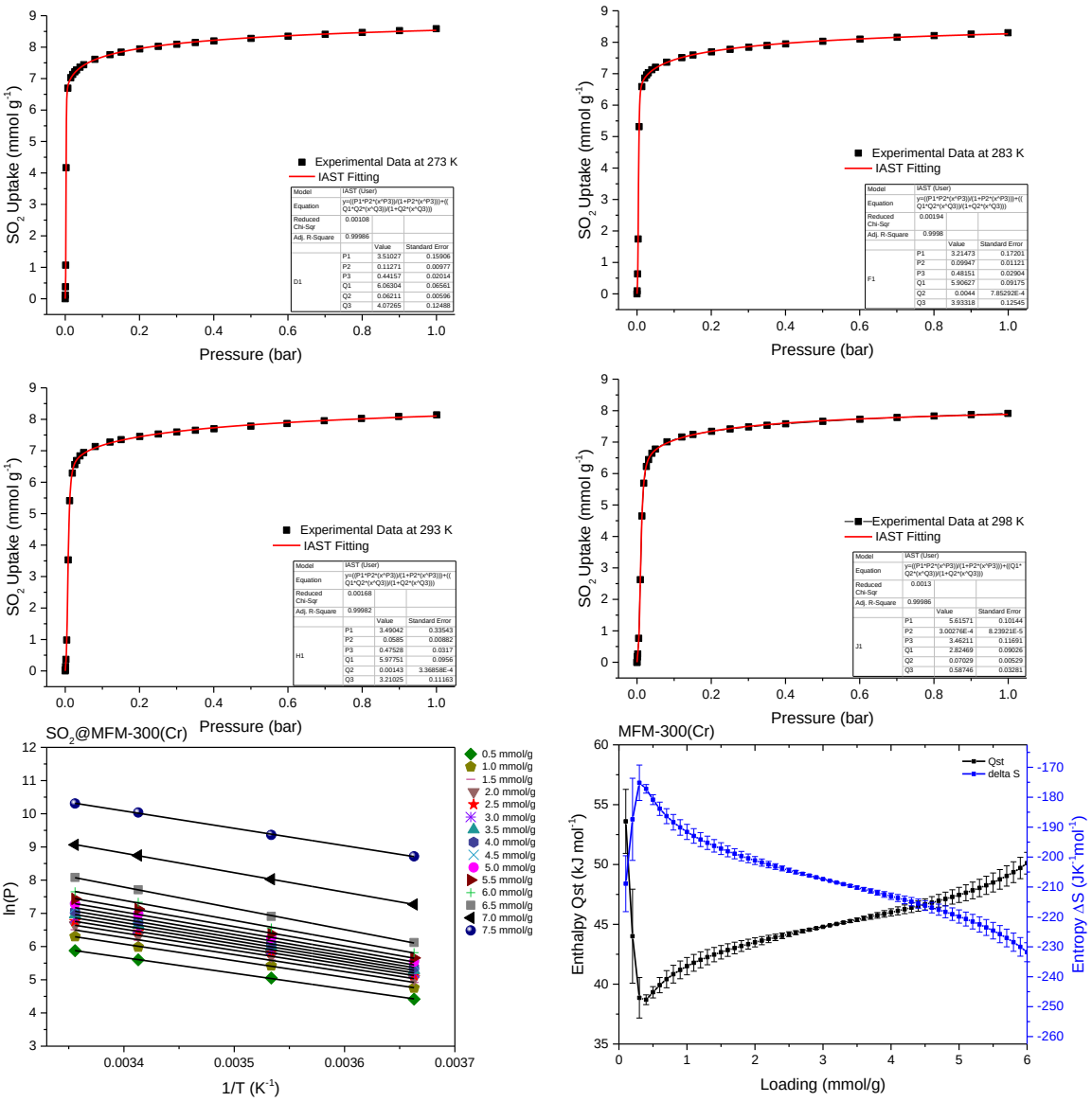

Figure S8: Fitting of isotherm by Dual-Site Langmuir Freundlich model for SO_2-loaded MFM-300(Cr) at 273, 283, 293 and 298 K up to 1 bar. Van't Hoff linear fittings and respective plots for Q_{st} and ΔS.

Table S6: Thermodynamic parameters for SO_2 adsorption in MFM-300(Cr)

n mmol g^{-1}	Q_{st} kJ mol^{-1}	Q_{st} error kJ mol^{-1}	ΔS J K^{-1} mol^{-1}	ΔS error J K^{-1} mol^{-1}	R^2
0.5	39.32453	0.4687	-180.83113	1.63731	0.99957
1.0	41.50533	0.72516	-191.61843	2.5332	0.99908
1.5	42.66628	0.56286	-197.19839	1.96626	0.99948
2.0	43.49313	0.37813	-201.16461	1.32091	0.99977
2.5	44.17524	0.20124	-204.43117	0.70298	0.99994
3.0	44.79129	0.04475	-207.37298	0.15632	1
3.5	45.38697	0.1423	-210.2048	0.49709	0.99997
4.0	45.99899	0.30349	-213.09595	1.06018	0.99987
4.5	46.66875	0.46686	-216.23251	1.63088	0.9997
5.0	47.45945	0.63165	-219.89232	2.20655	0.99947
5.5	48.49683	0.79097	-224.61853	2.7631	0.9992
6.0	50.10825	0.90533	-231.81194	3.1626	0.99902
6.5	53.22477	0.77203	-245.7373	2.69693	0.99937
7.0	48.81431	0.26533	-239.23672	0.92689	0.99991

3.8 Fitting of Isotherms to the Dual-Site Langmuir Equation - MFM-300($Al_{0.67}Cr_{0.33}$)

CO_2@MFM-300($Al_{0.67}Cr_{0.33}$)

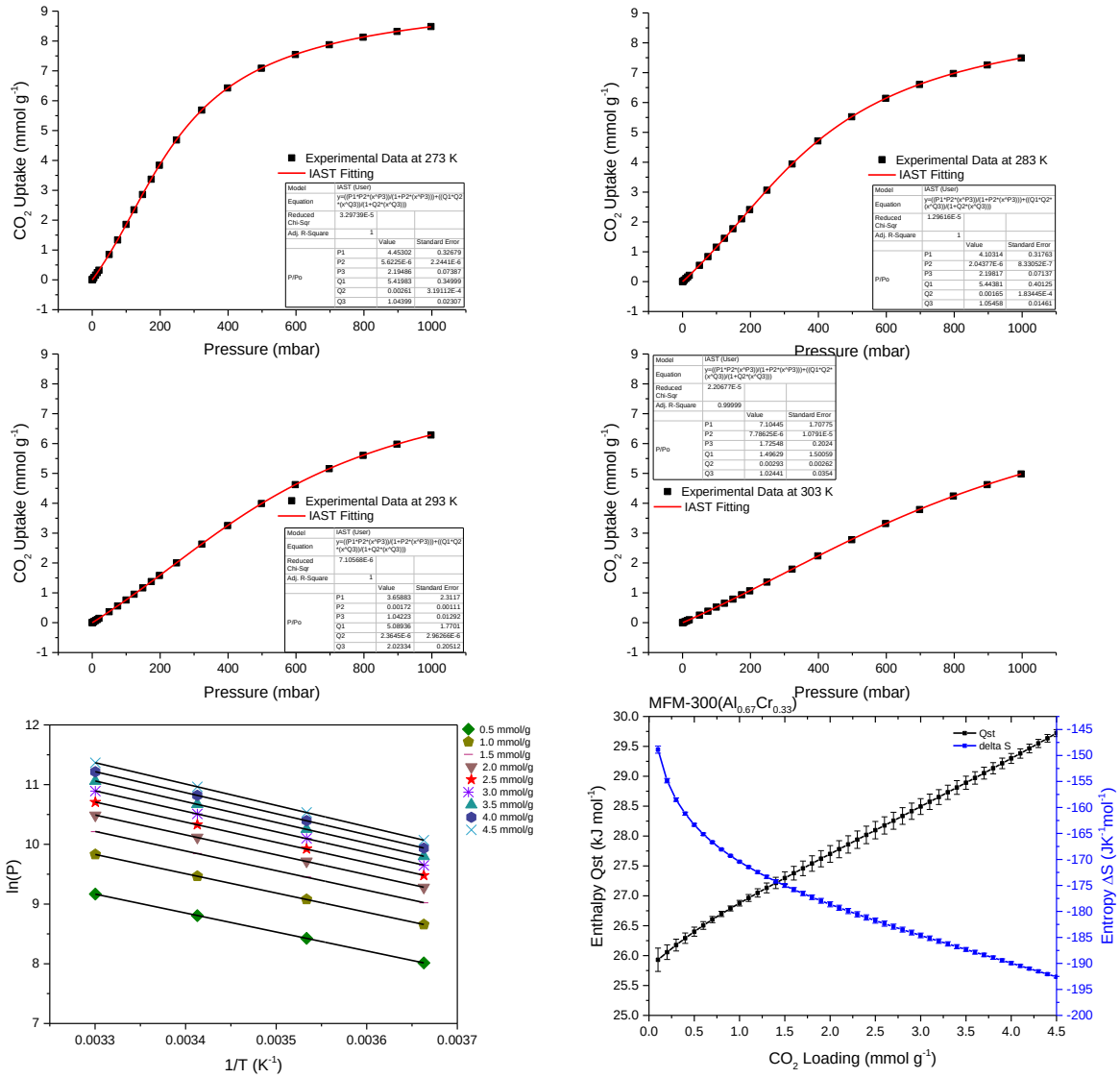

Figure S9: Fitting of isotherm by Dual-Site Langmuir Freundlich model for CO_2-loaded MFM-300($Al_{0.67}Cr_{0.33}$) at 273, 283, 293 and 303 K up to 1 bar. Van't Hoff linear fittings and respective plots for Q_{st} and ΔS.

Table S7: Thermodynamic parameters for CO_2 adsorption in MFM-300($Al_{0.67}Cr_{0.33}$)

n mmol g^{-1}	Q_{st} kJ mol^{-1}	Q_{st} error kJ mol^{-1}	ΔS J K^{-1} mol^{-1}	ΔS error J K^{-1} mol^{-1}	R^2
0.5	26.40059	0.07604	-163.33847	0.26462	0.99998
1.0	26.87749	0.04691	-170.43465	0.16324	0.99999
1.5	27.29735	0.10495	-175.01975	0.36525	0.99996
2.0	27.70065	0.13938	-178.63514	0.48506	0.99992
2.5	28.09811	0.14532	-181.76306	0.50572	0.99992
3.0	28.49382	0.13251	-184.61626	0.46113	0.99994
3.5	28.89188	0.10959	-187.31596	0.38138	0.99996
4.0	29.29822	0.08325	-189.94909	0.28973	0.99998
4.5	29.72178	0.05843	-192.59375	0.20335	0.99999

C_2H_2@MFM-300($Al_{0.67}Cr_{0.33}$)

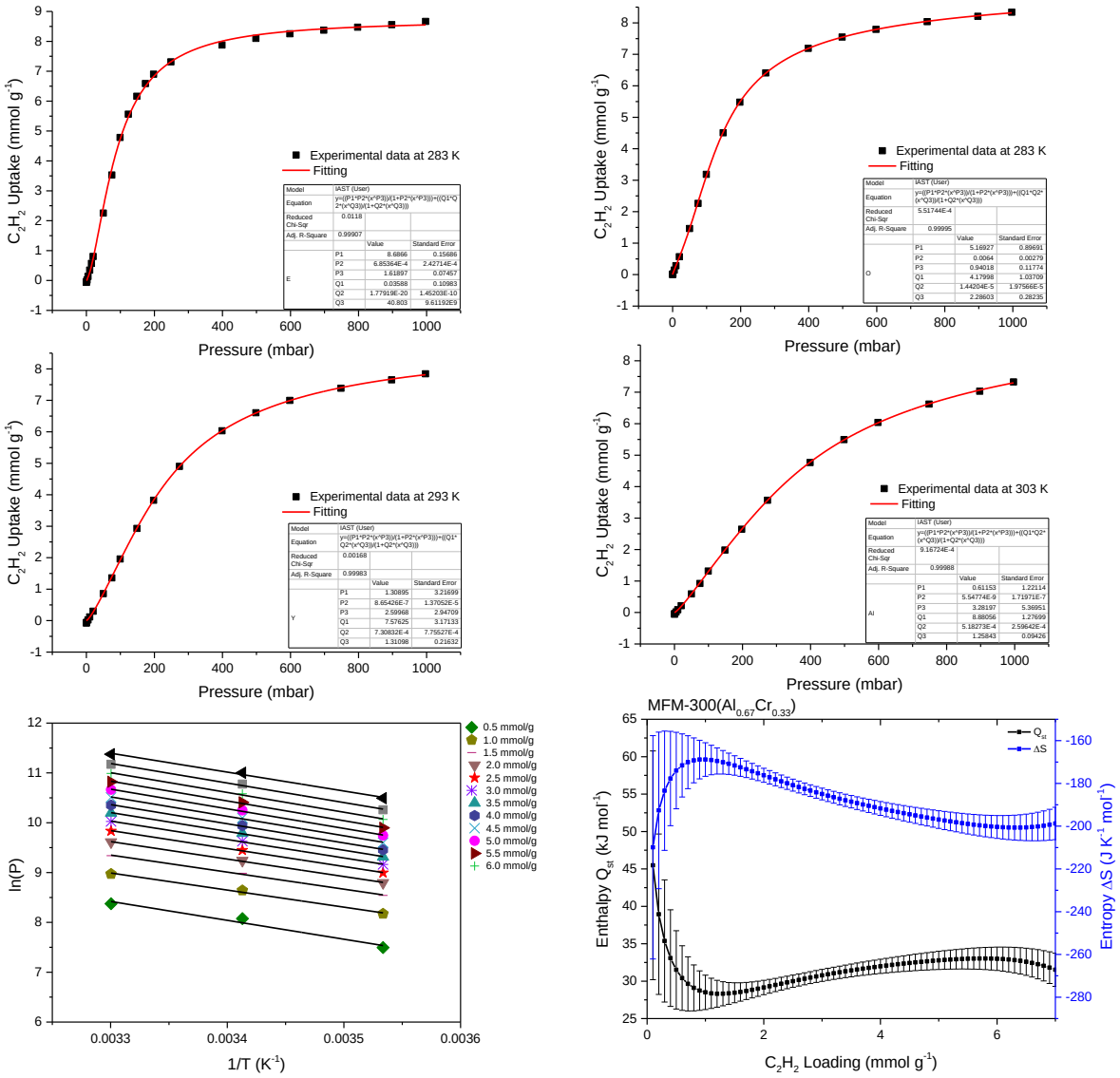

Figure S10: Fitting of isotherm by Dual-Site Langmuir Freundlich model for C_2H_2-loaded MFM-300($Al_{0.67}Cr_{0.33}$) at 273, 283, 293 and 303 K up to 1 bar. Van't Hoff linear fittings and respective plots for Q_{st} and ΔS.

Table S8: Thermodynamic parameters for C_2H_2 adsorption in MFM-300($Al_{0.67}Cr_{0.33}$)

n mmol g^{-1}	Q_{st} kJ mol^{-1}	Q_{st} error kJ mol^{-1}	ΔS J K^{-1} mol^{-1}	ΔS error J K^{-1} mol^{-1}	R^2
0.5	31.51108	5.23217	-173.99233	17.87808	0.94634
1.0	28.50482	2.29724	-168.8214	7.84954	0.98709
1.5	28.44797	1.33277	-168.8214	7.84954	0.99562
2.0	29.14989	0.96103	-176.18939	3.28378	0.99783
2.5	29.99313	0.822	-180.8113	2.80874	0.9985
3.0	30.77349	0.80095	-184.96992	2.73681	0.99865
3.5	31.43527	0.8517	-188.5757	2.91022	0.99853
4.0	31.98113	0.94783	-191.70493	3.23869	0.99824
4.5	32.42773	1.07136	-194.46578	3.6608	0.99782
5.0	32.77735	1.21253	-196.91027	4.14316	0.99727
5.5	32.9956	1.37191	-198.96393	4.68776	0.99655
6.0	32.99061	1.56278	-200.36068	5.33994	0.99552

SO_2@MFM-300($Al_{0.67}Cr_{0.33}$)

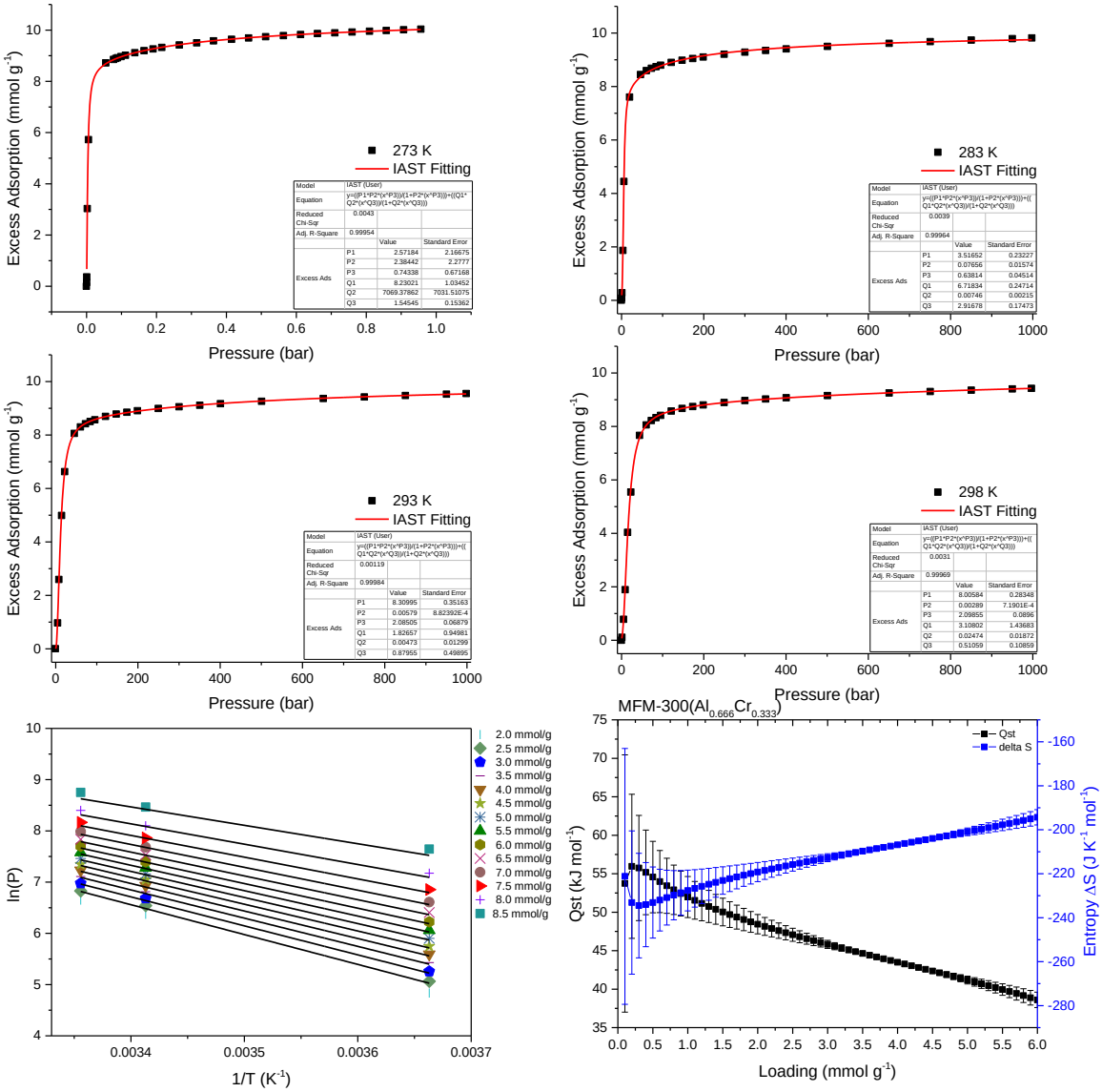

Figure S11: Fitting of isotherm by Dual-Site Langmuir Freundlich model for SO_2-loaded MFM-300($Al_{0.67}Cr_{0.33}$) at 273, 283, 293 and 298 K up to 1 bar. Van't Hoff linear fittings and respective plots for Q_{st} and ΔS.

Table S9: Thermodynamic parameters for SO_2 adsorption in MFM-300($Al_{0.67}Cr_{0.33}$)

n mmol g^{-1}	Q_{st} kJ mol^{-1}	Q_{st} error kJ mol^{-1}	ΔS J K^{-1} mol^{-1}	ΔS error J K^{-1} mol^{-1}	R^2
0.5	54.57291	4.64317	-233.10018	16.15725	0.98563
1.0	51.97112	2.66421	-227.65294	9.27088	0.99476
1.5	50.02587	1.79832	-223.08573	6.25777	0.99742
2.0	48.44281	1.25321	-219.23846	4.36092	0.99866
2.5	47.06781	0.84998	-215.83809	2.95775	0.99935
3.0	45.81712	0.52222	-212.71144	1.81721	0.99974
3.5	44.63832	0.23822	-209.74205	0.82894	0.99994
4.0	43.49365	0.02	-206.8419	0.0696	1
4.5	42.3516	0.26422	-203.93475	0.91942	0.99992
5.0	41.18147	0.50337	-200.94413	1.75161	0.9997
5.5	39.94845	0.74537	-197.78144	2.59371	0.9993
6.0	38.60711	0.99836	-194.32974	3.47407	0.99866
6.5	37.09044	1.27177	-190.41573	4.42549	0.99765
7	35.2877	1.57653	-185.75512	5.48598	0.99602
7.5	32.99787	1.91846	-179.84826	6.67584	0.99326
8.0	29.87872	2.22969	-171.98916	7.75885	0.98892

3.9 PXRD diffractograms

MFM-300(Cr)

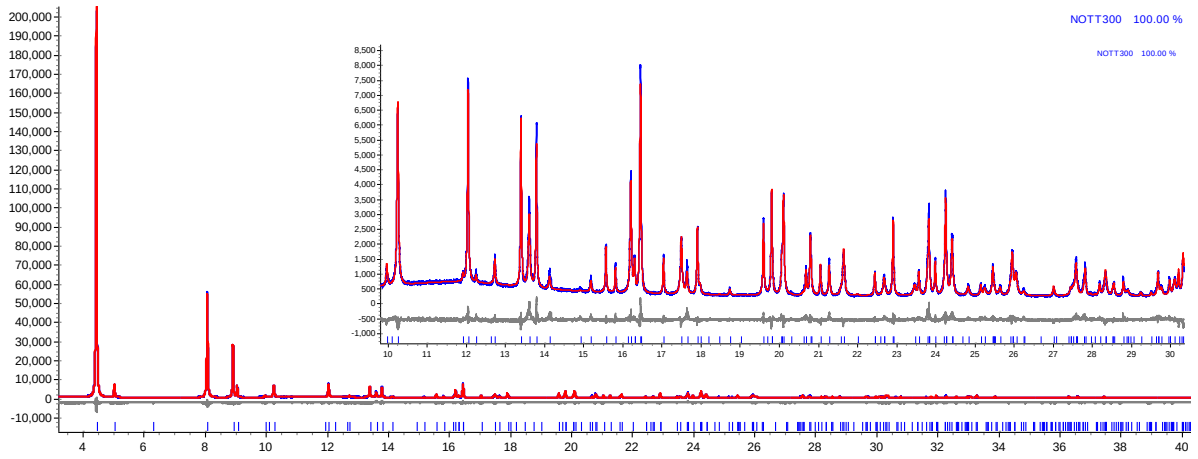

Figure S12: PXRD diffractogram of activated MFM-300(Cr). Experimental data shown in blue, Rietveld refinement model in red, difference pattern in grey.

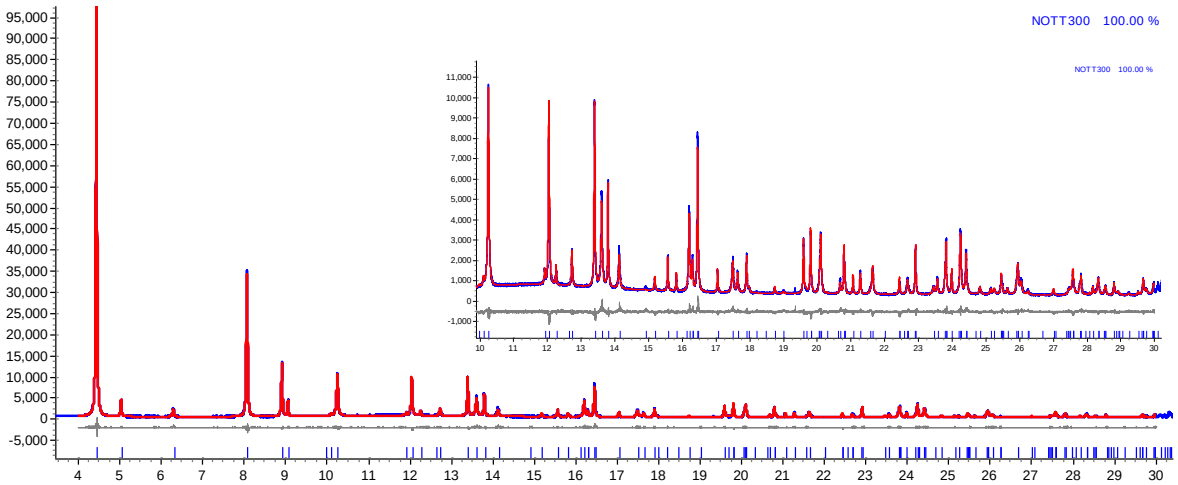

Figure S13: PXRD diffractogram of CO_2-loaded MFM-300(Cr). Experimental data shown in blue, Rietveld refinement model in red, difference pattern in grey.

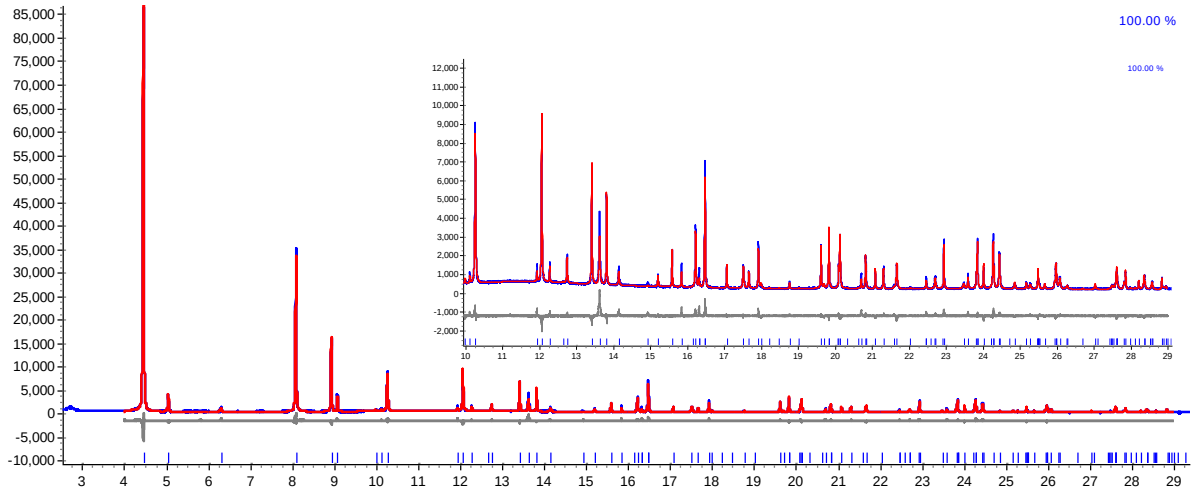

Figure S14: PXRD diffractogram of C_2H_2-loaded MFM-300(Cr). Experimental data shown in blue, Rietveld refinement model in red, difference pattern in grey.

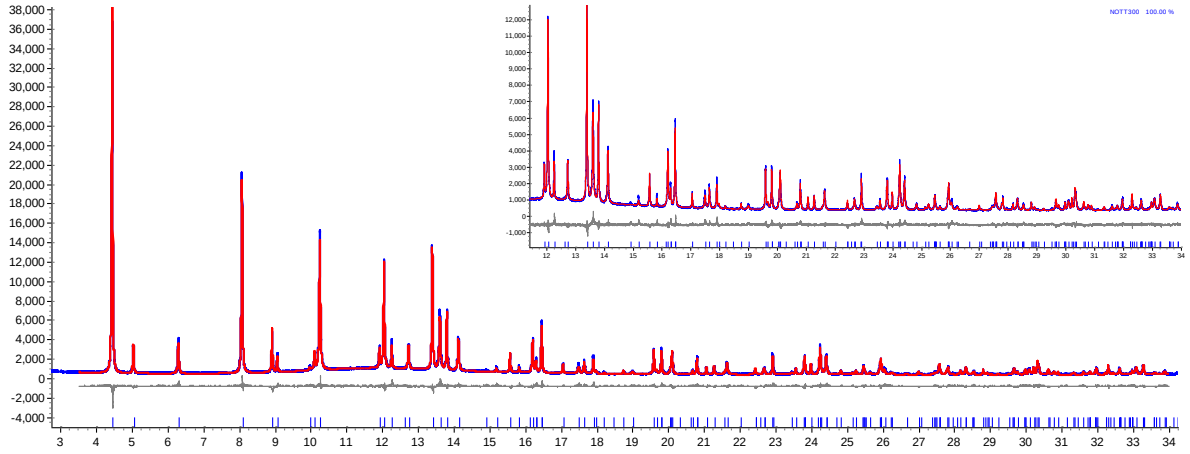

Figure S15: PXRD diffractogram of SO_2-loaded MFM-300(Cr). Experimental data shown in blue, Rietveld refinement model in red, difference pattern in grey.

MFM-300($Al_{0.67}Cr_{0.33}$)

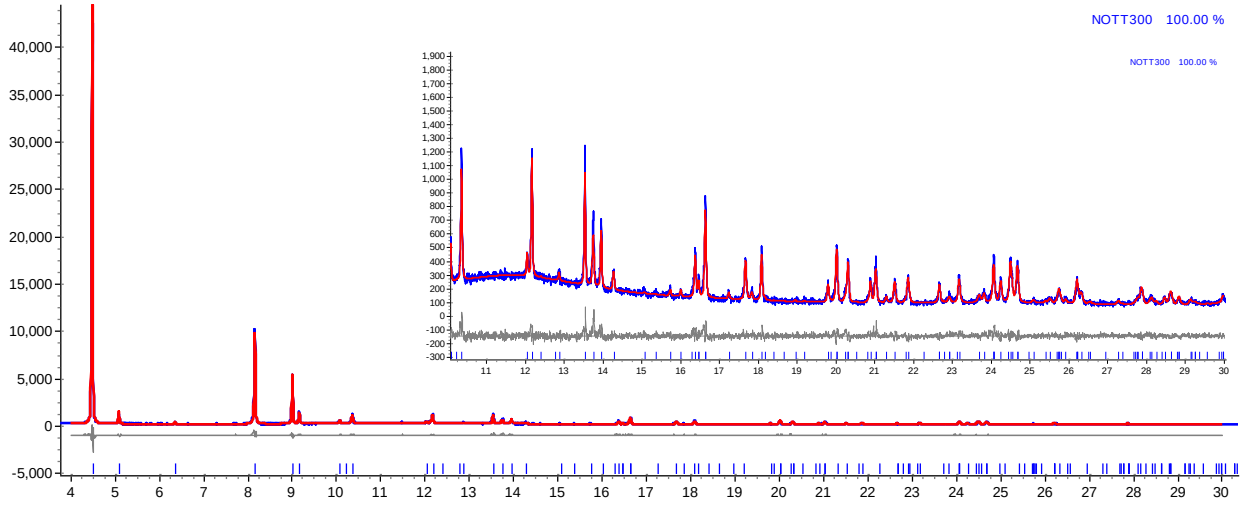

Figure S16: PXRD diffractogram of activated MFM-300($Al_{0.67}Cr_{0.33}$). Experimental data shown in blue, Rietveld refinement model in red, difference pattern in grey.

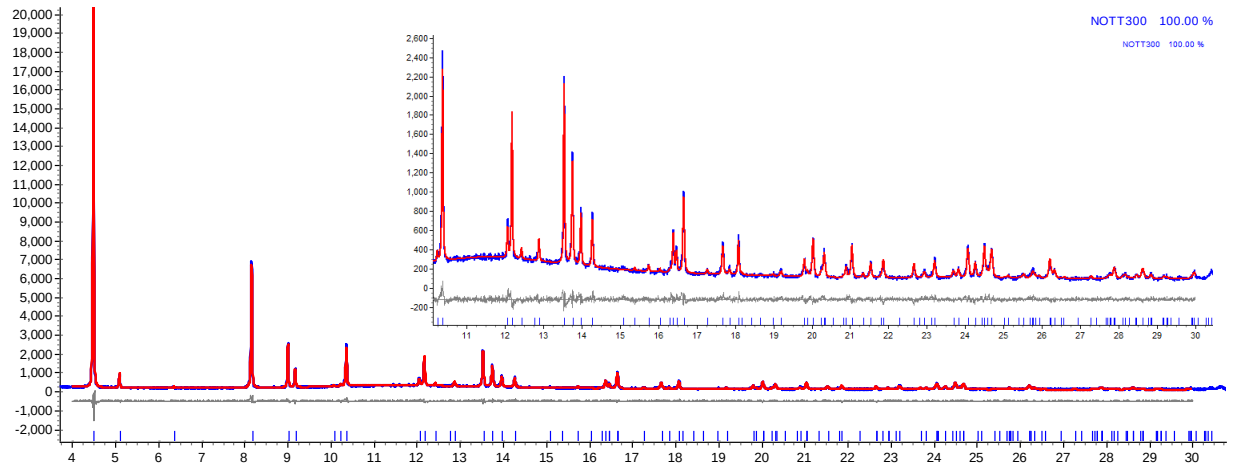

Figure S17: PXRD diffractogram of CO_2-loaded MFM-300(($Al_{0.67}Cr_{0.33}$). Experimental data shown in blue, Rietveld refinement model in red, difference pattern in grey.

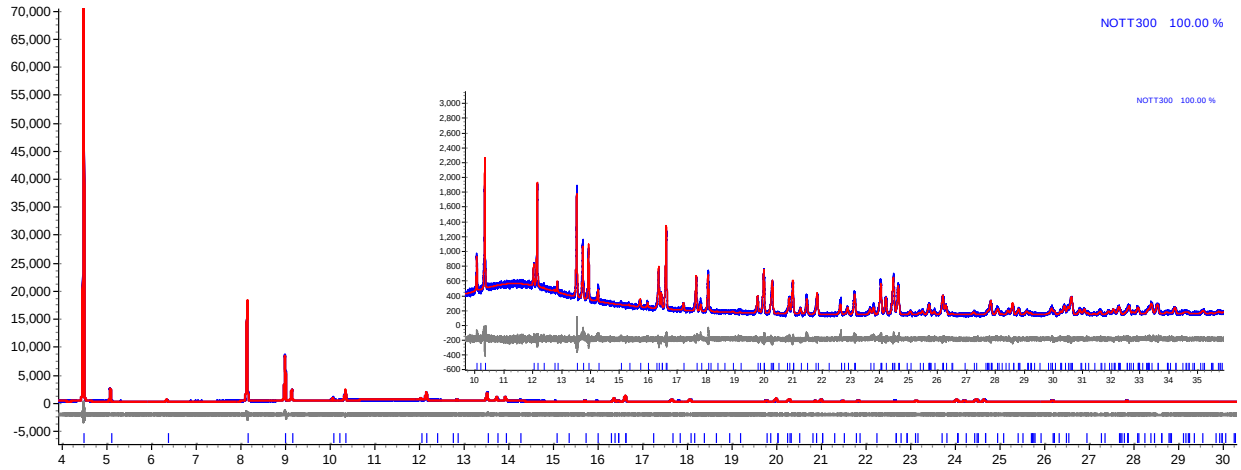

Figure S18: PXRD diffractogram of C_2H_2-loaded MFM-300(($Al_{0.67}Cr_{0.33}$). Experimental data shown in blue, Rietveld refinement model in red, difference pattern in grey.

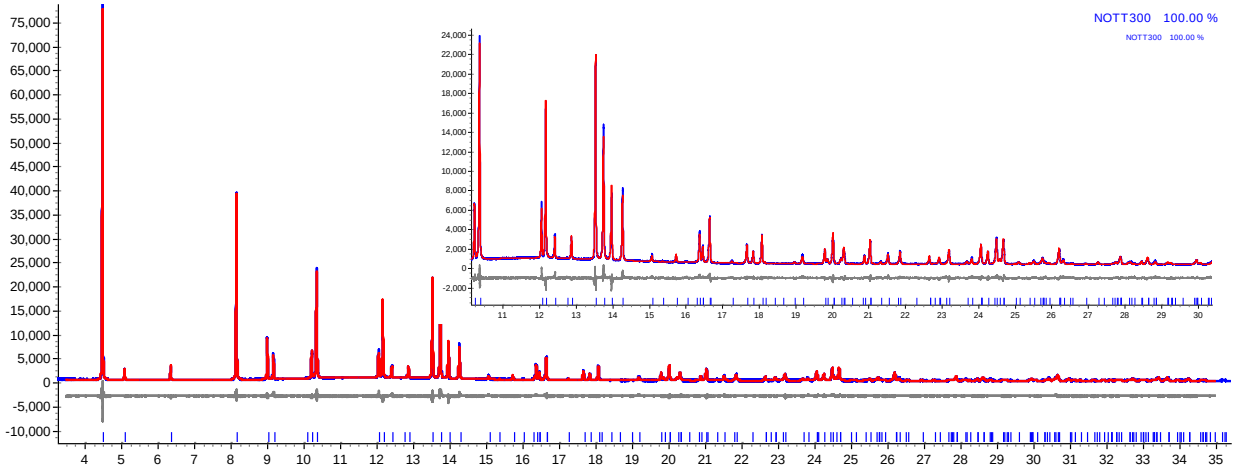

Figure S19: PXRD diffractogram of SO_2-loaded MFM-300(($Al_{0.67}Cr_{0.33}$). Experimental data shown in blue, Rietveld refinement model in red, difference pattern in grey.

3.10 Additional discussion on adsorption uptake

Table S10. Adsorption uptake presented as gas molecules per metal ion at 273 K and 1.0 bar

Gas/metal ion	MFM-300(Cr)	MFM-300($Al_{0.67}Cr_{0.33}$)	MFM-300(Al)
CO_2	1.71	1.83	1.45
C_2H_2	1.79	1.87	1.42
SO_2	1.99	2.15	1.68

4 References

1. X. Lin, I. Telepeni, A. J. Blake, A. Dailly, C. M. Brown, J. M. Simmons, M. Zoppi, G. S. Walker, K. M. Thomas, T. J. Mays, P. Hubberstey, N. R. Champness and M. Schröder, *J. Am. Chem. Soc.*, 2009, **131**, 2159–2171.

2. A. L. Myers and J. M. Prausnitz, *AIChEJ.*, 1964, **11**, 121–127.